Structural performance and analytical modelling of hybrid pine-poplar glulam beams through efficient use of resources

Carlos Cruz[a*], Rafael Bravo[a], Francisco J. Rescalvo[a], Yaiza Fuentes-García[a], Francisco J. Lafuente-Bolívar[b]

[a] Department of Structural Mechanics. UIMA Laboratory University of Granada. Campus de Fuentenueva s/n. 18071. Granada, Spain. carlos.cruz@ugr.es

[b] Department of Architectural and Engineering Graphic Expression. UIMA Laboratory. University of Granada. Campus de Fuentenueva s/n. 18071. Granada, Spain.

* Corresponding author

Keywords:

Resource efficiency, glulam beams, analytical formulation, pine, poplar, non-destructive testing.

Abstract:

This paper presents an experimental and analytical study on the structural performance and resource efficiency of hybrid glulam beams manufactured from pine (*Pinus nigra*) and poplar (*Populus × euramericana, clone MC*). In hybrid glulam beams, the modulus of elasticity is inherently non-uniform, varying both longitudinally and transversely because individual boards exhibit spatial stiffness variability along their length and across the cross-section. The main objective is to quantify the mechanical benefits of pine-poplar hybridization and to develop a predictive formulation for the beam modulus of elasticity accounting for these longitudinal and transverse stiffness distributions. Single-species and hybrid glulam beams were manufactured from pine and poplar boards and characterized by non-destructive testing and four-point bending tests according to UNE-EN 408. A new analytical formulation was developed to predict the beam modulus of elasticity from the spatial distribution of board elastic moduli, explicitly considering the strategic placement of the highest-stiffness boards in the outer lamellas, where bending stresses are maximum. The results show that this selection and placement increases the modulus of elasticity of hybrid glulam beams by 21%, reaching values comparable to single-species pine beams, while also increasing flexural strength by 18% and reducing beam density by 22%. These findings are relevant for both researchers and the structural timber industry, enabling efficient, lightweight, and competitive hybrid glulam solutions for structural applications.

1. Introduction

The use of timber in structural applications has gained renewed interest in recent years, especially within the context of sustainable building construction. This resurgence is due to its low environmental impact, capacity for CO_2 storage, versatility in design, and high mechanical efficiency relative to its weight [1–4]. Among the wide variety of engineered

wood products (EWPs), glulam beams are valued for their superior mechanical performance compared to solid sawn timber [5–7]. Their manufacturing process allows the combination of lamellas distributed according to strength and stiffness criteria [8–11]. It also eliminates defects through finger-jointed connections and enables the production of large-span elements with more uniform properties. This technology can maximize resource, structural, and economic efficiency of glulam beams by integrating lamellae of different qualities [12–14].

Traditionally, species such as *Pinus nigra* (PN) have been widely used in structural applications due to their high strength and stiffness. However, their mechanical heterogeneity, mainly due to the presence of knots, can limit their structural performance [15,16]. The increasing demand for forest resources has led to growing interest in fast-growing species such as *Populus × euramericana* or MC poplar (MC) [17,18] (where MC refers to its breeder Carlo Mellone, who obtained it in 1954 in Crescentino, Italy) particularly in hybrid solutions that combine different wood species to achieve an optimal balance between mechanical properties and density [19,20]. In hybrid configurations, pine is placed in the outer layers (where stresses are highest) and poplar is used in the core. PN wood in Spain is normally classified as C30 or higher (visual grade for the most demanding small-dimension structural timber - ME1) [21,22], with values of modulus of elasticity above 12000 MPa and a characteristic bending strength of 30 MPa and higher [23]. While poplar is classified as a hardwood for visual grading, with a strength class of T10 [24], it has traditionally been undervalued for structural purposes, but it offers advantages such as short rotation period, lower density (370 kg/m^3), and bending strength comparable to that of pine, with a modulus of elasticity around 8000 MPa [25]. Poplar MC, usually harvested at 9-15 years, reaches suitable dimensions for structural applications in a much shorter period than most conifers, which are typically cut at 30-50 years. In the case of slower-growing hardwoods such as oak or beech, rotation periods can even exceed 60–80 years.

Given the increasing demand for forest resources and the shorter rotation periods of poplar, several studies have explored the viability of using poplar in glued laminated beams as well as other engineered wood products. For example, [26] demonstrated that despite its lower stiffness, poplar can achieve bending strength values similar to or even higher than those of other species like spruce, particularly in laminated configurations [20], where thin lamellas are glued together to optimize the mechanical performance of the final member. The works of [24] and [27] focused on local Spanish cultivars and reported the good homogeneity and ductility of poplar versus the more brittle behavior of pine. More recent research has confirmed that hybrid glulam configurations can take advantage of the individual mechanical benefits of each wood type [28]. In particular, the strategic use of stiffer species in the outer layers can compensate for the lower stiffness of the core without compromising overall strength [29].

Numerous studies have shown that an appropriate arrangement of lamellas can significantly enhance the mechanical performance of glulam beams. Hybrid glulam configurations have been shown to increase bending strength by up to 20% [30] and [31], with comparable results to those obtained by reinforcing poplar lamellas with carbon fibers [32]. These improvements can be evaluated by correlating non-destructive

techniques such as longitudinal vibration tests and static bending tests [33]. However, most of the existing literature has focused on coniferous species, leaving a significant gap in the understanding of fast-growing hardwoods like poplar and eucalyptus [34]. Furthermore, current standards regulate glulam manufacturing. However, hybrid configurations require analytical models capable of accounting for spatial heterogeneity of mechanical properties. The authors have previously developed analytical formulations to estimate the modulus of elasticity of single-species, hybrid, and reinforced glulam beams, assuming uniform properties in the longitudinal direction and variation across the cross-section [25,35].

The aim of this work is to present a comprehensive methodology for the design, characterization, and analytical modeling of hybrid glulam beams combining *Pinus nigra* and MC poplar (*Populus × euramericana*), with a focus on maximizing resource efficiency and mechanical performance by strategically combining lamellas with different stiffnesses. The objectives of this study are to: 1) determine the mechanical properties of the constituent materials and the structural performance of single-species and hybrid glulam beams through non-destructive testing and four-point bending tests; 2) identify the effect of stiffness-based board selection and strategic placement (particularly placing higher-stiffness pine boards in the outer, most stressed zones) on the global stiffness and weight of the beams; and 3) calculate the global modulus of elasticity of the glulam beams by developing and validating a new analytical model based on the longitudinal and transverse spatial distribution of the moduli of elasticity of the boards.

2. Materials and methods

2.1 Origin, sawing, and drying of timber

For the manufacturing of single and hybrid-species glulam beams, two locally sourced wood species were used: pine (*Pinus nigra*, PN) and poplar (*Populus x euramericana,* MC cultivar). Specifically, the poplar wood was obtained from the MC cultivar harvested in the Vega of Granada (Spain). Pine was extracted from the Monte de Navahondona, located in the Natural Park of the Sierras de Cazorla, Segura y las Villas (Spain). The selected trees had trunk diameters of 310 and 550 mm, and approximate ages of 10 and 180 years for poplar and pine, respectively.

The experimental study was carried out in three consecutive phases: I) mechanical characterization of sawn timber; II) manufacturing of single-species and hybrid glulam control beams; III) design and fabrication of hybrid glulam beams aimed at maximizing resource efficiency. Phases I and II provided data on mechanical behavior pre- and post-gluing. Based on these results, hybrid pine-poplar beams were designed and manufactured in Phase III, improving resource efficiency by carefully selecting pine boards for the outer lamellae. In contrast, the poplar boards were randomly arranged within the rest of the cross-section and along the length of the beams.

Timber was processed at a local sawmill to lengths of 2500 mm. The cross-sections were: phase I 85 × 145 mm^2; phases II and III 75 × 150 mm^2. After sawing, the timber was stored and dried under natural air conditions for six months to reach an average moisture

content of 11 ± 2% according to [36]. To minimize the risk of biotic agents and excessive deformations, the timber was protected from rainfall and sunlight (covered with tarp, stored indoors).

2.2. Experimental testing

2.2.1. Non-destructive testing: longitudinal resonance test

The longitudinal resonance test evaluates the dynamic modulus of elasticity in the longitudinal direction ($MoE_{dyn,l}$). It is based on the analysis of the natural vibration frequencies of the boards. This method relies on the basic principles of longitudinal vibration dynamics, assuming homogeneous geometric and mechanical properties along the specimen. A controlled hammer impact is applied at one end of the specimen, and the vibratory response is recorded at the opposite end with a microphone (T-bone MM-1, Thomann), as shown in Fig. 1 (left). The captured signal is recorded with a Picoscope® oscilloscope C80MS/s rate 4424 and analyzed using the BING software (Beam Identification by Non-Destructive Grading [37]). This software identifies the first natural frequency of vibration f_1, from which the dynamic modulus of elasticity in the longitudinal direction $MoE_{dyn,l}$ can be obtained using the density ρ_m and length L of the specimen as shown in Eq. (1):

$$MoE_{dyn,l} = \rho_m \cdot (2 \cdot f_1 \cdot L)^2 \quad (1)$$

Figure 1: NDT resonance tests: longitudinal

2.2.2 Four-point bending tests: evaluation of bending strength, stiffness, and ductility

Four-point bending tests were performed on both sawn timber and glulam beams, following the guidelines established in [38]. The tests were conducted using a MICROTEST® universal testing machine, model EM2/200, equipped with a 200 kN capacity electromechanical actuator (see Fig. 2).

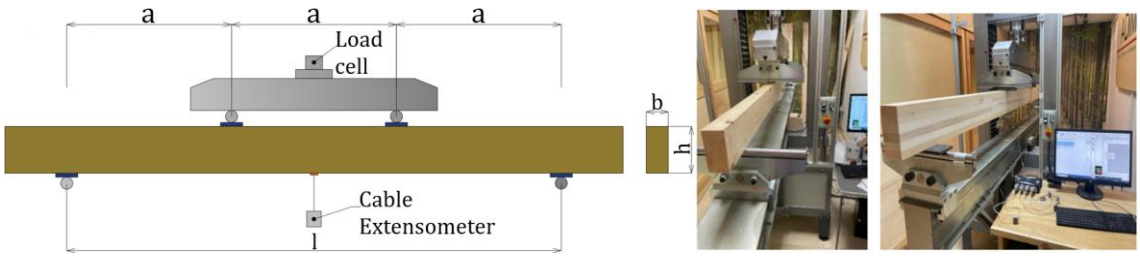

Figure 2: Four-point bending tests: boundary conditions and positioning of deflection measurement equipment (left), sawn timber (phase I, center), and control glulam beam (phase II, right).

The global static modulus of elasticity in bending MoE_{st} was computed at the load displacement (F-δ) curve between 10% (F_1-δ_1) and 40% (F_2-δ_2) at maximum load (F_{max}).

The calculation considered the beam cross-section, defined by width (*b*) and depth (*h*), as well as the distance (*a*) between the load application point and the nearest support (see Fig. 2). The displacements were recorded using a wire-type extensometer (ASM WS10) placed at mid-span (see Fig. 2 left). Equation (2) for MoE_{st} is:

$$MoE_{st} = \frac{3al^2 - 4a^3}{2bh^3\left(2\frac{\delta_2 - \delta_1}{F_2 - F_1} - \frac{6a}{5Gbh}\right)}, \quad (2)$$

where the shear modulus *G* used in this calculation was the G_{dyn} from previous non-destructive tests. The maximum bending strength, *MoR*, was calculated according to [38] using Eq. (3), where F_{max} represents the maximum load applied:

$$MoR = \frac{3F_{max}a}{bh^2}. \quad (3)$$

This expression assumes pure bending, linear elastic stress distribution across the section, and a rectangular cross-section. For hybrid beams, composite cross-section theory was applied using the transformed section method and parallel axis theorem (Steiner theorem) to compute *MoR*, considering the distribution of the elastic moduli in each lamella of the cross-section. Using this methodology, $MoR_{Steiner}$ is computed as:

$$MoR_{Steiner} = \frac{F_{max}a}{I_h}\frac{y_{gc}}{2}, \quad (4)$$

where y_{gc} is the position of the center of gravity of transformed (homogenized) cross-section transformed to pine and I_h is its corresponding inertia. This inertia is computed using the parallel axis theorem (Steiner theorem) as shown in Eq. (5):

$$I_h = \sum_{i=1}^{N_t}\left(\frac{1}{12}n_{mp}^i bt^3 + n_{mp}^i b\mathrm{t}\,(y^i - y_{gc})^2\right). \quad (5)$$

Here, t is the thickness of each lamella, $n_{mp}^i = MoE_m^i/MoE_p$ is the modular ratio between the moduli of elasticity of poplar and pine, and y^i is the centroid of each homogenized lamella. Strain gauges were also used to determine the stress-strain behavior of the specimens. Strain gauges (HBM K-CLY4, 10 mm grid length, X60 adhesive) were installed at mid-span on both the tension and compression faces.

Bending stiffness and ductility were determined from the load-displacement curves. Two stiffness values were evaluated according to [39]: the elastic stiffness $K_{1/3}$ and the ultimate stiffness K_{ult}, see Eq. (6):

$$K_{1/3} = \frac{F_{max}}{3\delta_{1/3}}; \quad K_{ult} = \frac{F_{max}}{\delta_{max}}, \quad (6)$$

where $\delta_{1/3}$ and δ_{max} are the mid-span displacements at 33% and 100% of the maximum load F_{max}, respectively. The difference between both stiffness values provides an indirect

indicator of ductile or brittle behavior. Ductility D_u was assessed using the geometric method defined in EN 12512:2001/A1:2005 [40], and is defined as shown in Eq. (7):

$$D_u = \frac{\delta_{max}}{\delta_y}, \tag{7}$$

where δ_y is the displacement at the elastic limit and δ_{max} is the displacement at maximum load. For more details on the calculation of δ_y and δ_{max} see references [32,41].

2.3. Analytical approach for the computation of the longitudinal modulus of elasticity of a glulam beam

This section presents an analytical formulation to estimate the longitudinal modulus of elasticity MoE_{an} of a glulam beam with spatially heterogeneous mechanical properties. The approach is based on elastic energy equivalence, combining the transformed section method (homogenization) and the parallel axis theorem. Consider a glulam beam composed of N_t lamellas across its cross-section and divided longitudinally into N_l sectors. Each lamella is indexed by the superscript i, and each longitudinal sector by j. The modulus of elasticity of a board i in sector j is denoted MoE^{ij}.

For an infinitesimal volume of the beam dV subjected to a longitudinal normal stress σ_x, the corresponding strain energy increment dU is given by Eq. (8):

$$dU = \frac{1}{2}\sigma_x \in_x dV = \frac{1}{2}\sigma_x \in_x dxdA\,. \tag{8}$$

The total strain energy per unit length in a cross-section belonging to sector *j* subjected to a bending moment M(x), which induces the strain $\in_x^{ij}(x)$ and stress $\sigma_x^{ij}(x)$ distributions, is expressed as shown in Eq. (9):

$$\frac{dU(x)}{dx} = \frac{1}{2}\sum_{i=1}^{N_t}\int_{A^{ij}} \sigma_x^{ij}(x) \in_x^{ij}(x) dA\,, \tag{9}$$

where $\sigma_x^{ij}(x) = \frac{n^{ij}M(x)}{I_h^i} y_h^i$ is the stress distribution in the board *j* of lamella i, $n^{ij} = \frac{MoE^{ij}}{MoE_h}$ is the modular ratio, I_h^j is the inertia of the homogenized cross-section, and y_h^{ij} is the distance of any point of the board *j* of the lamella i with respect to the centroid of the homogenized cross-section . Therefore, the strain is $\epsilon^{ij}(x) = \frac{\sigma_x^{ij}(x)}{MoE^{ij}}$, and the energy in the section is given by Eq. (10):

$$\frac{dU(x)}{dx} = \frac{1}{2}\sum_{i=1}^{N_t}\frac{{n^{ij}}^2 M(x)^2}{MoE^{ij}{I_h^j}^2}\int_{A^{ij}} {y^{ij}}_h^2\, dA = \frac{1}{2}\sum_{i=1}^{N_t}\frac{{n^{ij}}^2 M(x)^2 I^{ij}}{MoE^{ij}{I_h^j}^2} = \frac{M(x)^2}{2{I_h^j}^2}\sum_{i=1}^{N_t}\frac{{n^{ij}}^2 I^{ij}}{MoE^{ij}}\,. \tag{10}$$

The I_h^j is computed using the parallel axis theorem after some algebraic steps, as: $I_h^j = \sum_{i=1}^{Nt} n^{ij}\left(I^{*ij} + A^{ij}{d^{ij}}^2\right) = \frac{1}{MoE_h}\sum_{i=1}^{Nt} MoE^{ij}\left(I^{*ij} + A^{ij}{d^{ij}}^2\right) = \sum_{i=1}^{Nt} MoE^{ij} I^{ij}$, where I^{ij} and I^{*ij} are the inertias of each board with respect to the centroid of the homogenized section and to its own centroid respectively, A^{ij} is its area, and d^{ij} is the

distance between the centroid of the board and the neutral axis of the homogenized section. Therefore, the strain energy per unit length according to Eq. (11):

$$\frac{dU(x)}{dx}=\frac{M(x)^2}{2\sum_{i=1}^{Nt} MoE^{ij} I^{ij}}. \quad (11)$$

Integrating along the beam length, and taking into account that MoE^{ij} and I^{ij} are constant within each sector *j*, the total strain energy U^{tot} of the hybrid beam by Eq. (12) is:

$$U^{tot} = \int_0^L \frac{M(x)^2}{2\sum_{i=1}^{Nt} MoE^{ij} I^{ij}} dx = \sum_{j=1}^{N_l} \frac{A_M^j}{2\sum_{i=1}^{Nt} MoE^{ij} I^{ij}} = \sum_{j=1}^{N_l} U^j, \quad (12)$$

where $A_M^j = \int_{x^j}^{x^{j+1}} M(x)^2 dx$ is the area of $M(x)^2$ diagram over sector *j*, and U^j is the total energy of sector *j*. Where M(x) is given by Eq. (13), the moment distribution defined in the four-point bending test from [38]:

$$M(x) = \begin{cases} Px & 0 \le x < \frac{L}{3} \\ \frac{PL}{3} & \frac{L}{3} \le x < \frac{2L}{3} \\ P(L-x) & \frac{2L}{3} \le x \le \frac{L}{3} \end{cases}. \quad (13)$$

The total energy of a homogeneous beam, characterized by a modulus of elasticity MoE_{an}, is $U^{tot} = \frac{A_M}{2MoE_{an} I}$. Equating the total energy of the homogeneous and hybrid beams (previous and Eq. (13)), the following relation is obtained by Eq. (14):

$$\frac{A_M}{MoE_{an} I} = \sum_{j=1}^{N_l} \frac{A_M^j}{\sum_{i=1}^{Nt} MoE^{ij} I^{ij}}, \quad (14)$$

which is expressed in Eq. (15):

$$\frac{1}{MoE_{an} I} = \sum_{j=1}^{N_l} \frac{A_M^j}{A_M} \frac{1}{MoE^j I^j}. \quad (15)$$

On the right-hand side of Eq. (16), $MoE^j I^j = \sum_{i=1}^{Nt} MoE^{ij} I^{ij}$ is the equivalent flexural rigidity of the sector *j*. Using this relation, the modulus of elasticity MoE^j of a sector *j* can be computed using Eq. (16):

$$MoE^j = \frac{\sum_{i=1}^{Nt} MoE^{ij} I^{ij}}{I^j}, \quad (16)$$

which is maximum when the external lamellas, those having the highest I^{ij}, also have the highest MoE. Finally, the Eq. (16) can be expressed in compact form in Eq. (17):

$$\frac{1}{MoE_{an} I} = \sum_{j=1}^{N_l} C^j \omega^j, \quad (17)$$

where parameter $C^j = A_M^j / A_M$ is the ratio between the area of $M(x)^2$ at sector *j* and total area and works as a weight factor of $\omega^j = 1/MoE^j I^j$. This formulation reveals that the inverse of MoE_{an} is governed by a weighted summation of inverses of flexural rigidities of each sector, where C^j reflects the relative influence of each sector on MoE_{an}. Consequently, maximizing MoE_{an} requires the implementation of the following design principles that will be applied in Subsection 2.6:

1. Position of boards with higher modulus of elasticity in the outermost lamellas, where their contribution to the inertia is maximized.

2. Prioritize the placement of boards with the highest elastic moduli in segments with the highest bending moment, i.e., where the weighting factor C^j reaches its maximum.

2.4. Phase 1: Mechanical characterization of sawn timber

Using the vibration-based method described in Subsections 2.2.1, the dynamic longitudinal modulus of elasticity ($MoE_{dyn,l}$) was measured for 362 of *Pinus nigra* (PN) boards and 522 MC poplar boards (MC), see Fig. 3. For PN and MC, the mean and standard deviation values were 10885 ± 1823 MPa and 9377 ± 257 MPa, respectively, with associated confidence intervals of [9062-12708] MPa for PN and [9120-9634] MPa for MC. From these intervals, 25 specimens of each species (50 in total) were randomly selected for further mechanical characterization.

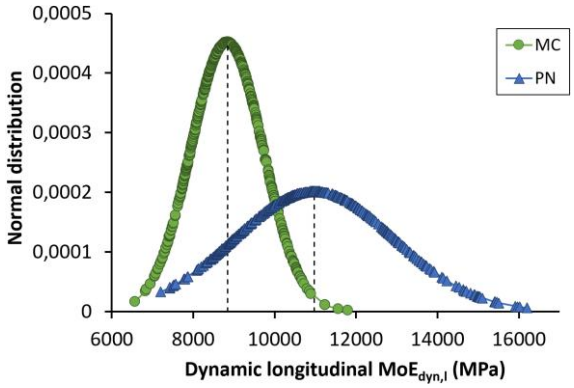

Figure 3: $MoE_{dyn,l}$ distribution for MC and PN.

The selected boards were machined to final dimensions of 60 × 120 mm² and a length of 2450 mm for static mechanical testing, which included four-point bending, compression, tension parallel to the grain, and compression perpendicular to the grain, in accordance with [38]. Table 1 compiles the results of these tests along with the values of density and the corresponding strength class, which was determined according to the [22].

Mechanical properties		**PN**		**MC**	
		Mean	**Std Dev**	**Mean**	**Std Dev**
Modulus of elasticity (MPa)					
Dynamic	$MoE_{dyn,l}$	10885	1823.5	9377	257.1
Static	MoE_{st}	10970	1514.2	8942	129.5
Strength (N/mm²)					

Bending	*MoR*	47.1	6.7	51.5	1.5
Tension parallel	$\sigma_{t,0}$	41.4	11.7	34.1	8.5
Compression parallel	$\sigma_{c,0}$	48.4	6.3	32.5	0.8
Compression perpendicular	$\sigma_{c,90}$	4.3	0.9	2.9	0.1
Density (kg/m³)					
Density	ρ_m	504	65.2	370	40.3

Table 1: Mechanical properties of PN and MC: mean and standard deviation of moduli of elasticity, strength, density, and strength class.

The results reveal significant differences between both species in terms of elastic and strength properties. The $MoE_{dyn,\ l}$ of PN is approximately 17% higher than that of MC, although it exhibits greater variability due to mechanical heterogeneity. Similarly, the static modulus MoE_{st} of PN exceeds that of MC by about 22%, with a consistent trend in the standard deviation. In general, dynamic moduli are higher than static ones, although in the case of PN, the presence of defects tends to reduce this difference.

With regard to strength and density properties, MC showed a 9.3% higher average bending strength *MoR* than PN, due to its lower presence of knots and lower standard deviations. However, PN was superior to MC in tensile strength $\sigma_{t,0}$, compressive strength parallel to grain $\sigma_{c,0}$, and compressive strength perpendicular to grain $\sigma_{c,90}$ by 21.5%, 48.9%, and 48.2%, respectively. The PN also had a 36% higher density than MC, hence reflecting its greater compactness. These results indicate that PN offers better mechanical behavior under axial loads, whereas MC stands out in bending applications, making it a valuable component for use in hybrid glulam beam designs. It is important to note that knots are removed during the lamination process, which reduces variability in the mechanical properties of glulam beams.

2.4.1 Selection of boards for phases 2 and 3

The results acquired from the non-destructive tests in Section 2.4 were used to select the timber boards for phases 2 and 3. Within the previously defined confidence intervals, 95 boards of *Pinus nigra* (PN) and 125 boards of MC poplar (MC) were randomly selected for manufacturing the control beams in both phases.

Four-point bending tests in the elastic range were carried out on 40% of the selected boards from each species. The main purpose of these tests was to establish a correlation formula between the longitudinal dynamic modulus of elasticity $MoE_{dyn,l}$, and the static modulus of elasticity MoE_{st} (see Fig. 4, left and right), a key element to obtain the MoE_{st} of the boards for the analytical formulation presented in subsection 2.3. The results show a higher dispersion in the correlation for PN ($R^2 = 0.57$) compared to MC ($R^2 = 0.74$), mainly due to the greater presence of defects in PN.

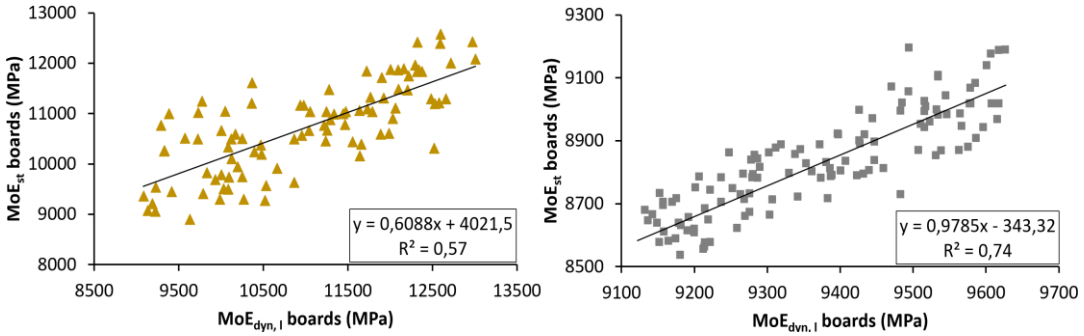

Figure 4: Correlation between the longitudinal dynamic modulus of elasticity $MoE_{dyn,l}$, and the static modulus of elasticity MoE_{st}, for sawn timber boards of PN (left) and MC (right).

2.5 Phase 2: Manufacturing of single-species and hybrid (control) glulam beams

Based on the boards selected in Subsection 2.4.1, a total of 30 finger-jointed glulam beams were manufactured, with a cross-section of 75 × 150 mm, 25 mm thick lamellas, and a length of 3000 mm. These included 10 single-species pine beams (PN_C), 10 single-species poplar beams (MC_C), and 10 hybrid beams: five control (PN-MC_C) and five designed for optimized resource efficiency (PN-MC_O). The finger joints had a length of 15 mm and a tooth pitch of 4 mm, complying with the geometric requirements specified in Annex I of the UNE-EN 14080 [42]. The specific arrangement of these joints within each lamella, as well as the final layout of the beams, is shown in Fig. 5. Final board lengths of 750 mm and 1125 mm were obtained after trimming the original boards of 2500 mm.

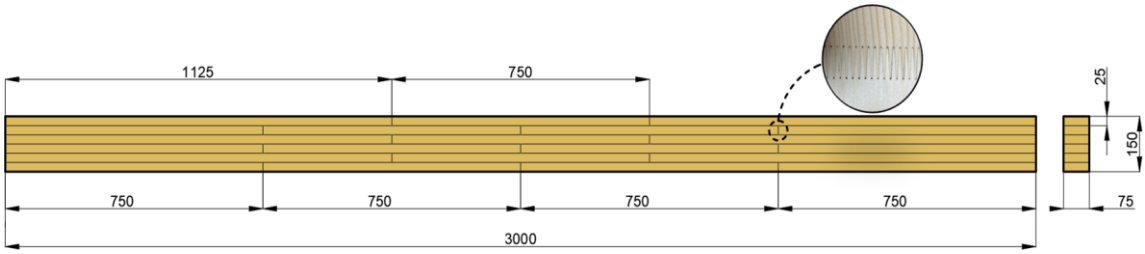

Figure 5: Final layout, dimensions of the glulam beams, and location of finger joints.

All beams were manufactured following the guidelines of UNE-EN 14080 [42]. The gluing process was carried out following the prescriptions in Annex I.5, using Loctite HB S709 PURBOND polyurethane adhesive. This adhesive, with a curing time of 175 minutes for a joint thickness of 0.1 mm and a workability time of 70 minutes, was applied under controlled conditions (20 °C ambient temperature, 65% relative humidity). The laminated beams were pressed using a Stromab SL2-3000. A pressure of 10 N/mm² was applied to the finger joints and 0.8 N/mm² between the lamellas. Throughout the manufacturing process, the moisture content of the wood was carefully monitored and maintained at an average value of 10 ± 1%. The specimens were manufactured at the UIMA laboratory of the University of Granada. Flexural strength tests were conducted on the finger joints, yielding a minimum strength of 33.8 MPa in the PN case.

2.6. Phase 3: Design and manufacturing of hybrid glulam beams for enhanced resource efficiency

The main objective of the resource efficiency maximization was to increase the static modulus of elasticity MoE_{st} of the hybrid control beams PN-MC_C, so that the PN-MC_O

beams exhibit moduli closer to those of the single-species pine beams PN_C. Using the analytical model presented in Subsection 2.3, the modulus of elasticity of the hybrid beams was enhanced with a focus on maximizing resource efficiency by selectively improving specific boards, particularly those belonging to the lamellas highlighted in red in Fig. 6.

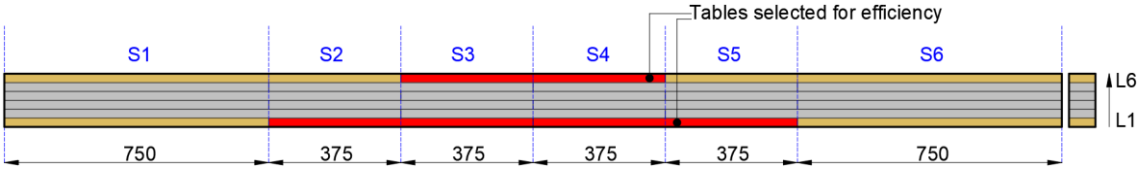

Figure 6: Structural layout of the hybrid glulam beam made of pine (yellow) and poplar (grey) divided into sectors. Red boards represent the lamellas specifically chosen to improve the modulus of elasticity of the glulam beam through targeted enhancement of their MoE_{st}.

The targeted boards were located in the zones experiencing the highest tensile and compressive stresses: the outermost upper and lower lamellas (section-wise), and the central third of the beam (span-wise), see Fig. 6. Taking into account the position of the finger joints, which represent changes in board properties within each lamella, the beam was divided into six sectors (S1-S6). The boards selected to maximize resource efficiency on the upper (compression) side were located in sectors S3 and S4, while those on the lower (tension) side were located in sectors S2 to S5.

The selected boards only represented 6% of the total volume of the beam, while the rest of the boards were randomly selected. Therefore, the strategy focused on maximizing resource efficiency by enhancing the modulus of elasticity where it is most structurally relevant (boards in red), without significantly increasing the overall weight of the beam.

3. Experiments and analysis of results

3.1 Experimental and analytical evaluation of single-species control glulam beams (PN_C and MC_C)

Non-destructive tests, destructive bending tests, and analytical calculations were carried out on the single-species control glulam beams PN_C and MC_C (10 of each type) to compute the following properties: longitudinal dynamic modulus of elasticity $MoE_{dyn,l}$, static modulus of elasticity MoE_{st}, analytical modulus of elasticity MoE_{an}, elastic stiffness $K_{1/3}$, ultimate stiffness K_{ult}, ductility D_u, bending strength MoR, density ρ_m, and strength class (R means Refused). Tables 2 and 3 present the results for the PN_C and MC_C beams, respectively. The data show that PN_C beams exhibit superior mechanical properties compared to MC_C beams. The characteristic flexural strength values of both species [43] were comparable: 40 MPa for PN_C beams, exceeding the requirements of the GL24h strength class, and 33 MPa for MC_C beams, which also meet the criteria of the GL20h strength class, in accordance with EN 14080 [42].

Beams	$MoE_{dyn,l}$ (MPa)	MoE_{st} (MPa)	MoE_{an} (MPa) (var. respect to MoE_{st} in %)	$K_{1/3}$ (kN/m)	K_{ult} (kN/m)	D_u	MoR (MPa)	Density (kg/m³)	SC
PN_C_1	12087	11589	11607 (0%)	775	642	1.09	56	532	GL24h
PN_C_2	12323	11975	11631 (-3%)	823	774	1.07	59	531	GL24h
PN_C_3	12444	11631	12133 (+4%)	818	788	1.05	48	548	GL24h
PN_C_4	11561	10401	11002 (+5%)	709	693	1.04	40	537	GL20h
PN_C_5	12787	11498	11702 (+2%)	771	706	1.11	59	541	GL22h
PN_C_6	12174	12179	12330 (+1%)	828	749	1.12	59	502	GL26h
PN_C_7	12983	11859	11715 (-1%)	814	764	1.1	43	500	GL24h
PN_C_8	11924	11732	12046 (+3%)	643	738	1.06	50	522	GL24h
PN_C_9	12156	11706	11791 (+1%)	793	779	1.02	52	571	GL24h
PN_C_10	12471	11356	11471 (+1%)	785	764	1.04	45	531	GL22h
Mean	**12291**	**11593**	**11742 (+1%)**	**776**	**740**	**1.06**	**51**	**532**	**GL24h**
SD	**411**	**481**	**372**	**55**	**44**	**0.03**	**7**	**21**	

Table 2: Mean Mechanical Properties and Standard Deviation of Single-Species Pine Control Glulam Beams (PN_C).

Beams	$MoE_{dyn,l}$ (MPa)	MoE_{st} (MPa)	MoE_{an} (MPa) (var. respect to MoE_{st} in %)	$K_{1/3}$ (kN/m)	K_{ult} (kN/m)	D_u	MoR (MPa)	Density (kg/m³)	SC
MC_C_1	9457	8950	10003 (+11%)	620	532	1.21	50	387	GL20h
MC_C_2	9589	8995	9621 (+7%)	614	562	1.12	48	390	GL20h
MC_C_3	9487	9306	10218 (+9%)	655	583	1.15	50	389	GL20h
MC_C_4	9618	9440	10587 (+11%)	706	526	1.29	56	390	GL20h
MC_C_5	9543	9219	9418 (+2%)	633	576	1.11	33	384	GL20h
MC_C_6	9383	9017	8892 (-1%)	616	586	1.05	44	387	GL20h
MC_C_7	8994	8957	8666 (-3%)	618	508	1.27	54	390	GL20h
MC_C_8	9530	9190	9381 (+2%)	631	590	1.08	42	387	GL20h
MC_C_9	9563	9652	10619 (+9%)	670	564	1.24	54	395	GL20h
MC_C_10	9821	9727	10472 (+7%)	661	576	1.19	51	392	GL20h
Mean	**9499**	**9245**	**9788 (+6%)**	**642**	**560**	**1.17**	**49**	**389**	**GL20h**
SD	**212**	**284**	**665**	**28**	**27**	**0.08**	**7**	**3**	

Table 3: Mean Mechanical Properties and Standard Deviation of Single-Species Poplar Control Glulam Beams (MC_C).

The values obtained from the non-destructive tests were slightly higher than those from the destructive ones, as the former do not account for lamella interfaces or finger joints. A similar conclusion applies to the analytical modulus of elasticity MoE_{an}, which showed values close to or slightly above MoE_{st} as indicated by the percentage differences in the table.

Compared to MC_C, PN_C beams showed higher values in all stiffness-related properties and *MoR*, although they had lower ductility and a smaller difference between $K_{1/3}$ and K_{ult}, indicating more brittle behavior. The MC_C beams exhibited smaller standard deviations due to the greater homogeneity of the poplar. Notably, both types of beams achieved similar bending strengths (51 MPa for PN_C and 49 MPa for MC_C, respectively), highlighting the good structural performance of MC. The PN_C beams had a 37% higher average density than MC_C, despite poplar being a hardwood species. The greater variability in pine density is attributed to its natural imperfections. It is worth noting the substantial improvement in the MoE_{st} of pine glulam beams compared to sawn timber (see Table 1), with an average increase of 5.68%. This increase results from the reduction of natural heterogeneities through the lamination process (the previous

value was 10970 MPa). In contrast, the improvement for poplar was around 3.3%. Fig. 7 (left) shows the load-displacement envelopes and mean curve from the four-point bending tests of the 10 PN_C (blue) and 10 MC_C (green) beams. Fig. 7 (right) displays the stress-strain curves obtained from strain gauges installed on the tension side. In both Figures, the PN_C beams show a steeper slope due to their higher stiffness. The maximum load reached by PN_C beams was 42 kN (mean: 40 kN), compared to 40 kN (mean: 36 kN) for MC_C beams. Despite these differences, the MC_C beams displayed a ductile elastoplastic behavior, in contrast to the linear-elastic and brittle response observed in PN_C beams. This was confirmed by ductility values calculated according to EN 12512:2001 [40]. Fractures in PN_C beams occurred in tension (Fig. 8, left), while MC_C beams failed in a more ductile manner (Fig. 8, right).

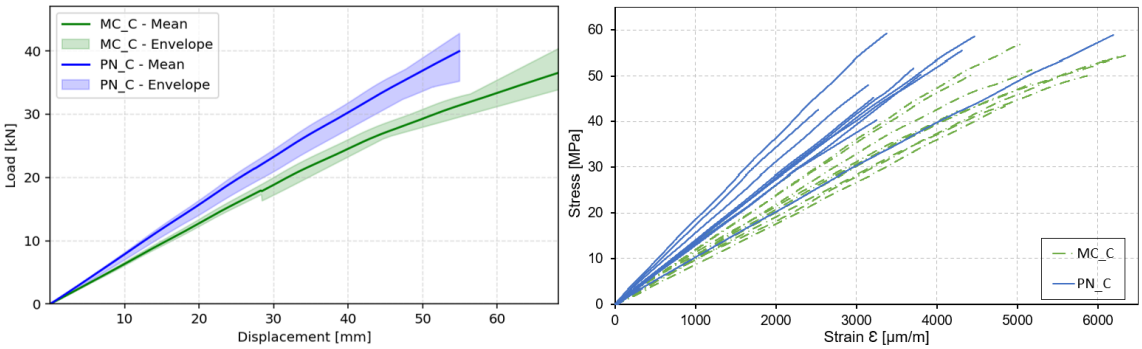

Figure 7: Load-Displacement envelope and mean curve for control glulam beams MC_C and PN_C (left). Stress-Strain curves (right).

Figure 8: Failure mode of PN_C Beam (left) and MC_C Beam (right).

3.2 Experimental and analytical evaluation of control hybrid glulam beams (PN-MC_C)

Five control hybrid glulam beams PN-MC_C were tested, in which the pine timber used for the lamella boards were randomly selected. Table 4 summarizes the mechanical properties obtained from destructive and non-destructive tests, as well as those calculated using the analytical model and the strength classification (R means Refused). When compared to the results in Table 3, the control hybrid beams PN-MC_C showed improved stiffness and elastic moduli relative to the poplar single-species beams MC_C, with increases of *7%* in $MoE_{dyn,l}$, 7% in MoE_{st}, 5.5% in MoE_{an}, and 8% in $K_{1/3}$, 15% in K_{ult}, and -7% in D_u.

Beams	$MoE_{dyn,l}$ (MPa)	MoE_{st} (MPa)	MoE_{an} (MPa) (var. respect to MoE_{st} in %)	$K_{1/3}$ (kN/m)	K_{ult} (kN/m)	D_u	MoR (MPa)	$MoR_{Steiner}$ (MPa)	Density (kg/m³)	SC
PN-MC_C_1	10551	9704	9980 (+3%)	689	628	1.11	53	58	382	R
PN-MC_C_2	10223	10485	10715 (+7%)	730	669	1.12	50	54	409	GL22c
PN-MC_C_3	10033	9681	10444 (+8%)	689	626	1.10	49	52	415	R
PN-MC_C_4	9828	9618	10423 (+8%)	681	644	1.08	48	51	409	R
PN-MC_C_5	10569	9768	10020 (+3%)	674	645	1.08	49	53	422	R
Mean	**10241**	**9851**	**10316 (+5%)**	**693**	**642**	**1.09**	**50**	**53**	**407**	**R**
SD	**323**	**169**	**170**	**19**	**16**	**0.02**	**2**	**3**	**15**	
Var. respect MC_C	**7%**	**7%**	**5.5%**	**8%**	**15%**	**-7%**	**2%**	**8%**	**5%**	
Var. respect PN_C	**-17%**	**-15%**	**-12%**	**-10.7%**	**-13.3%**	**3%**	**-2%**	**1%**	**-24%**	

Table 4: Mean mechanical properties and standard deviation of control hybrid glulam beams PN-MC_C. R symbol in SC means Refused (MoE_{st} < 10400 MPa, below the minimum required for GL20c according to UNE-EN 14080 [42] combined classes).

Since the PN-MC_C beams are composed of timber with differing mechanical properties, the bending strength was calculated both assuming a homogeneous cross-section (MoR, Eq. (3)) and a hybrid cross-section using the Steiner method ($MoR_{Steiner}$, Eq. (4)), based on the $MoE_{dyn,l}$ values in the mid-section. The mean bending strength increment compared to the MC_C beams was 2% under the homogeneous assumption and 8% when applying the hybrid approach. These improvements were achieved with only a modest 5% increase in the density.

However, despite these gains, the performance of the PN-MC_C beams remained notably below that of the pine single-species beams PN_C, with reductions of 17% in $MoE_{dyn,l}$, 15% in MoE_{st}, 12% in MoE_{an}, 10.7% in $K_{1/3}$, 13.3% in K_{ult}, 2% in MoR, and a marginal 1% in $MoR_{Steiner}$, all of which are accompanied by a 24% lower density and an increase of 3% in D_u. In addition, when assigning the glulam strength class according to UNE-EN 14080 [42] (combined lay-up), most PN-MC_C beams do not reach the minimum mean stiffness required for GL20c (MoE_{st} < 10400MPa) and are therefore labeled as 'R' (Refused) in Table 4. The observed reduction is consistent with tensile failures in the outer pine lamella near mid-span associated with inherent defects (Figure 9), where stresses are highest.

Figure 9: Failure of the PN-MC_C beam caused by defects in the pine.

3.3 Experimental and analytical analysis of maximizing resource efficiency in hybrid glulam beams (PN-MC_O)

Five hybrid glulam beams designed to maximize resource efficiency PN-MC_O were tested. In this case, the pine timber used for the outer lamella boards was selected from samples exhibiting the highest modulus of elasticity, as shown in Fig. 3. Table 5 summarizes the elastic moduli, stiffness, ductility, bending strength, density, and

strength class of each beam, along with their mean values and standard deviations. In general, these values are higher than those for the hybrid control beams.

Beams	$MoE_{dyn,l}$ *(MPa)*	MoE_{st} *(MPa)*	MoE_{an} *(MPa) (var. respect to* MoE_{st} *in %)*	$K_{1/3}$ *(kN/m)*	K_{ult} *(kN/m)*	D_u	*MoR (MPa)*	$MoR_{Steiner}$ *(MPa)*	*Density (kg/m³)*	*SC*
PN-MC_O_1	10809	11292	11448 (+1.4%)	721	631	1.20	57	54	405	GL24c
PN-MC_O_2	11244	11592	11469(+1.1%)	770	693	1.13	58	57	404	GL24c
PN-MC_O_3	11334	11417	11611 (+1.7%)	776	699	1.14	61	58	432	GL24c
PN-MC_O_4	11077	11535	11753 (+1.9%)	781	719	1.11	55	58	413	GL24c
PN-MC_O_5	11276	11794	11908 (+1.0%)	792	692	1.18	62	58	403	GL24c
Mean	**11148**	**11526**	**11638 (+1.0)**	**768**	**687**	**1.12**	**59**	**57**	**412**	**GL24c**
SD	**212**	**169**	**194**	**25**	**30**	**0.01**	**3**	**3**	**12**	
Var. respect MC_C	**15%**	**21%**	**16%**	**16%**	**18%**	**-4%**	**18%**	**14%**	**6%**	
Var. respect PN_C	**-11%**	**-1%**	**-1%**	**-1%**	**-1%**	**-8%**	**16%**	**11%**	**-22%**	

Table 5: Values of $MoE_{dyn,l}$, MoE_{st}, MoE_{an}, $K_{1/3}$, K_{ult}, D_u, MoR, $MoR_{Steiner}$, density, and strength class SC of the hybrid glulam beams designed to maximize resource efficiency *PN-MC_O*.

Significant improvements in the performance of PN-MC_O beams were observed in comparison to PN-C beams, evidenced by reductions of 11% in $MoE_{dyn,l}$, 1% in MoE_{st}, 1% in MoE_{an}, 1% in $K_{1/3}$, 1% in K_{ult}, and a 22% reduction in density. Conversely, certain mechanical properties of the beams designed to maximize resource efficiency surpassed those of the PN-C beams, with increases of 2% in MoR and 11% in $MoR_{Steiner}$. It is noteworthy that this enhanced performance was achieved by modifying only 12.5% of the total timber volume.

Table 6 summarizes the mean values and standard deviations of the elastic moduli, stiffness, ductility, bending strength, and average density for the control hybrid beams PN-MC_C, the hybrid beams designed to maximize resource efficiency PN-MC_O, and the pine single-species beams PN_C. The beams designed to maximize resource efficiency achieved the following average increases of over the PN-MC_C beams: 8.9% in $MoE_{dyn,l}$, 12.8% in MoE_{st}, 12.0% in MoE_{an}, 10.8% in $K_{1/3}$, and 7.0% in K_{ult}. The bending strength MoR increased significantly by 18% under the homogeneous hypothesis, while the increase using the Steiner method was more modest. Notably, the density increase remained minimal (approximately 1.7%). Compared to the PN_C beams, the resource-efficient hybrid beams showed smaller performance differences, indicating that the mechanical behavior of PN-MC_O beams closely approximates that of the pine beams with a decrease of 22% in density. It is also worth noting that the dynamic and static modulus values are quite similar within each of these beams, whereas the analytical modulus tends to be slightly higher, as it assumes rigid lamella interfaces and does not account for the presence of finger joints.

		PN-MC_C		PN-MC_O		PN_C	
Elastic properties (N/mm²)		***Mean***	***SD***	***Mean (var. respect to PN-MC_C in %) (var. respect to PN_C in %)***	***SD***	***Mean***	***SD***
Longitudinal dynamic modulus of elasticity	$MoE_{dyn,\ l}$	10241	323	11148 (+8.9%) (-9.3%)	189	12291	411
Static modulus of elasticity	MoE_{st}	9851	365	11526 (+12.8%) (-0.5%)	452	11593	481
Analytical modulus of elasticity	MoE_{an}	10316	87	11638 (+12.0%) (-0.8%)	174	11742	372
Elastic stiffness	$K_{1/3}$	693	19	768(+10.8%) (-1.0%)	25	776	55
Ultimate stiffness	K_{ult}	642	16	687(+7.0%) (-7.1%)	30	740	44
Ductility	D_u	1.09	0.02	1.12	0.01	1.06	0.03
Strength properties (N/mm²)							
Bending	MoR	50	2	59 (+18.0%) (+15%)	3.0	51	7
Bending	$MoR_{Steiner}$	53	3	57(+1.8%) (+15%)	3	-	-
Density (kg/m³)							
Density	ρ_m	407	15	412 (+1.7%) (-22%)	12	532	21

Table 6: Summary of the mechanical properties of hybrid and pine beams.

Fig. 10 shows the envelope and mean curves of the load-displacement relations (left) and stress-strain curves (right), respectively, for the PN_C (blue), control hybrid PN-MC_C (magenta), and hybrid beams designed to maximize resource efficiency PN-MC_O (yellow) beams. Three groups of curves are distinguishable in the left and right figures: the PN-MC_C beams, with the lowest slope; the PN_C beams, with the steepest slope but also the highest variability; and finally, the PN-MC_O beams, which show slightly lower slopes than PN_C but with less dispersion. All beams exhibited brittle linear-elastic behavior with minimal plastic range. Notably, as shown in Fig. 10 (left), the PN-MC_O and PN_C beams reached similar maximum loads (38 kN and 40 kN, respectively), while the PN-MC_C beams reached around 34 kN. The lower variability in the PN-MC_O beams is attributed to the homogenizing effect of the poplar.

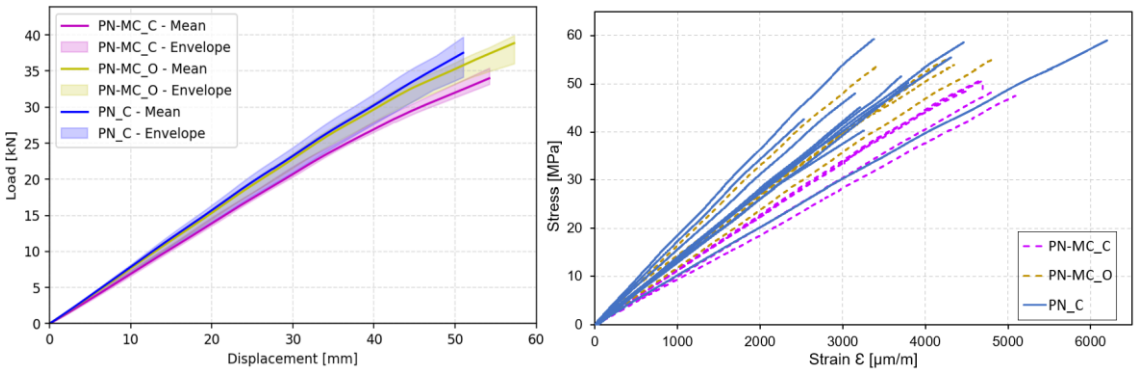

Figure 10: Load-displacement envelope and mean curve for hybrid beams *PN-MC_C* and *PN-MC_O* (left). Stress-strain curves for control single-species beams *PN_C* (blue), control hybrid beams *PN-MC_C* (magenta), and the hybrid beams designed to maximize resource efficiency PN-*MC_O* (yellow), (right).

As shown in Fig. 10 (right), the highest bending strength corresponded to the PN-MC_O beams, reaching an average *MoR* of 59 ± 3 MPa, representing an 18% increase over the PN_C beams under the homogeneous hypothesis, with comparable results under the Steiner approach. This enhancement is attributed to high-quality pine used in the zones of maximum tensile and compressive stress, and to the fact that failure occurred in the timber itself rather than at the finger joints (see Fig. 11). In contrast, the PN_C and PN-MC_C beams showed similar bending strengths (51 ± 8 MPa and 50 ± 2 MPa,

respectively). The brittle behavior was also reflected in the ductility values, calculated according to EN 12512:2001 [40]. These values also reflect this brittle behavior.

Figure 11: Failure of a *PN-MC_O* Beam by fracture in the pine boards.

Using Eq. (17) from Subsection 2.3, the modulus of elasticity was estimated for each sector of the hybrid beams. Fig. 12 shows the distribution of MoE_{an} across the six sections (S1–S6) of a control hybrid beam (PN-MC_C, in orange and top beam) and a hybrid beam designed to maximize resource efficiency (PN-MC_O, in blue and bottom beam), calculated based on the MoE_{st} of each board. The improvement in the elastic modulus of the central external pine boards of 18% in the top lamella and 26% in the bottom, led to a 13-15% increase in the modulus of elasticity in the central span of the beam (where the material enhancement was applied), representing 12.5% of the total volume of the beam. As a result, the elastic moduli increased between 8.9% and 13%, as reflected in Table 6.

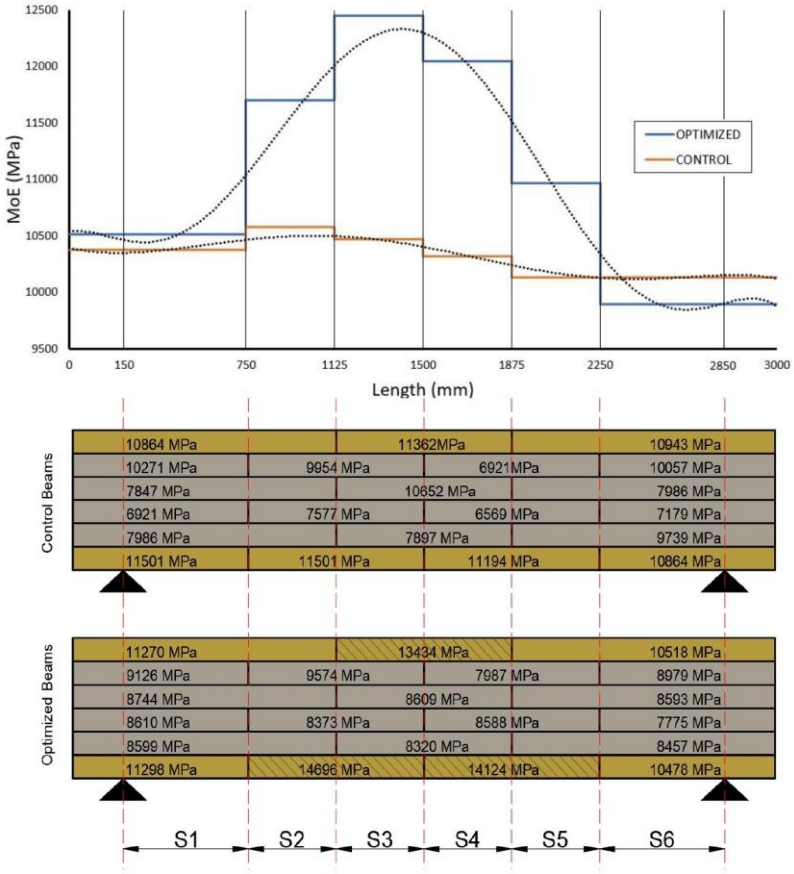

Figure 12: Analytical Modulus of elasticity (MoE_{an}) distribution along hybrid glulam beams. Top graph compares control (orange) and beams designed to maximize resource efficiency (blue). Below, MoE_{st} of individual boards per section is shown for each beam type, highlighting stiffness improvements.

3.4 Parametric analysis of hybrid glulam beams designed to maximize resource using the analytical formulation

To validate the experimental results obtained through the targeted pine boards, a parametric analysis was performed using the analytical formulation described in Subsection 2.3. This analysis evaluated how the analytical modulus of elasticity MoE_{an} changes as a function of the static modulus of elasticity MoE_{st} of the selected pine boards.

Fig. 13 illustrates the MoE_{an} for a hybrid PN-MC beam as the MoE_{st} of the selected boards increases. The horizontal lines correspond to the average MoE_{an} of PN-MC_C (10434 MPa, lower line) and the average MoE_{an} of PN_C (11742 MPa, upper line). Using the correlation for PN boards in Fig. 4, the range of MoE_{st} used in this analysis is between 11000 and 15000 MPa. The graph shows a linear trend: as the MoE_{st} of the pine targeted boards increases, the MoE_{an} of the hybrid beam increases. For instance, with a MoE_{st} of 14270 MPa in the selected pine boards, the resulting MoE_{an} reaches 11742 MPa and matches the average modulus of the PN_C beams. This implies that a relative increase of 21% in the MoE_{st} of the selected pine boards enables the hybrid beam to achieve the same modulus as the single-species pine beams. Moreover, if the MoE_{st} is increased to 15000 MPa, the beam would achieve an MoE_{an} of approximately 12000 MPa.

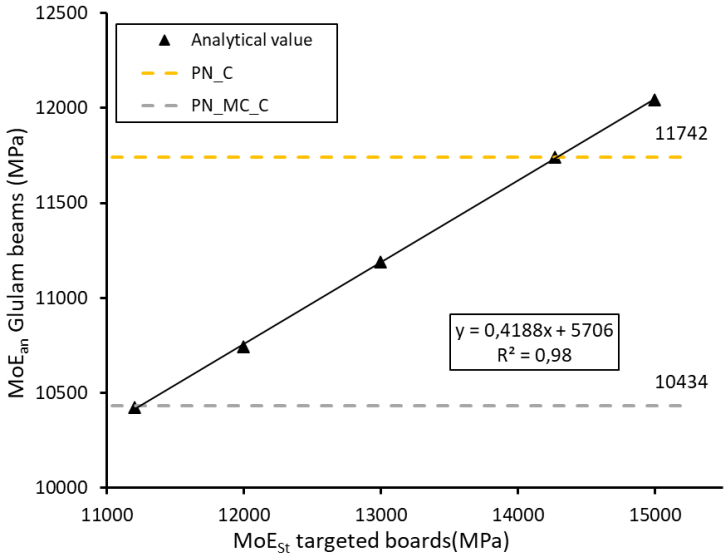

Figure 13: Correlation between MoE_{st} at targeted pine boards and MoE_{an} at hybrid *PN_MC* glulam beams designed to maximize resource efficiency.

4. Conclusions

The experimental and analytical results presented in this study highlight the structural potential of hybrid glulam beams composed of *Pinus nigra* and poplar (*Populus × euramericana*, cultivar MC). The experimental program (non-destructive testing and four-point bending tests) confirmed that hybrid beams designed to maximize resource

efficiency attained static modulus of elasticity values comparable to those of single-species pine beams and showed an 18% higher bending strength compared to the control hybrid beams. Additionally, the non-destructive testing methods correlated well with static test results, supporting their potential integration into structural grading processes.

The results also demonstrate the effect of stiffness-based board selection and strategic placement. In particular, placing high elastic modulus boards of pine lamellas in the outer tensile and compressive zones of the beams (where bending stresses are maximum) increased the global modulus of elasticity without a substantial increase in overall weight. This improvement results in a 22% reduction in density compared to pine beams, confirming the efficiency of the multi-species design for flexural applications by modifying only 12.5% of the volume of the boards in the beam.

Finally, the analytical formulation showed good agreement with experimental results, estimating the modulus of elasticity of the beam by accounting for the longitudinal and cross-sectional distribution of the mechanical properties of the boards comprising the lamellas, with relative deviations below 5%. Moreover, the analytical model demonstrated that a 21% increase in the static modulus of selected pine boards is sufficient for the hybrid beams to match or exceed the mechanical performance of single-species pine beams. This makes the model a valuable tool for the efficient design of hybrid glulam beams, enabling material selection and design improvements without the need for full-scale testing.

In general, the study emphasizes the value of poplar as a structurally viable component in hybrid glulam beams. Its low density, combined with bending strength comparable to pine, makes it suitable for lightweight, high-performance hybrid configurations. The results provide a solid experimental and analytical basis for the structural use of multispecies glulam, promoting sustainable construction by combining timbers with different mechanical qualities and supporting resource-efficient design for structural applications.

Funding

This work was supported by the SMARTTIMBER project "*Productos estructurales inteligentes de madera multiespecie para construcción industrializada baja en carbono*", PID2020.114386RB.I00; the LIGHTTIMBER project "*Cajones estructurales de madera técnica aligerada para una construcción de baja huella ecológica*", TED2021-130039B-I00; and the GLUCAR project "Pine-poplar-carbon fibre mixed glulam beams of high performance with laminated optimized by using artificial intelligence", PID2023-148379OA-I00.

Author Statement

Carlos Cruz: Formal analysis, experimental test, writing – original draft. Rafael Bravo: Conceptualization, supervision, formal analysis, writing – review & editing. Francisco J. Rescalvo: Conceptualization, methodology, investigation. Yaiza Fuentes: Formal analysis, data curation, writing – original draft. Francisco J. Lafuente: Conceptualization, supervision, investigation.

Declaration of Competing Interest

The authors declare that they have no known competing financial interests or personal relationships that could have appeared to influence the work reported in this paper.

Bibliography

[1] Huang H, Su S, Li L. Advancing timber construction: historical growth, research frontiers, and time series forecasting. J Asian Archit Build Eng 2024:1–30. https://doi.org/10.1080/13467581.2024.2373829.

[2] De Araujo V. Timber construction as a multiple valuable sustainable alternative: main characteristics, challenge remarks and affirmative actions. Int J Constr Manag 2023;23:1334–43. https://doi.org/10.1080/15623599.2021.1969742.

[3] Petruch M, Walcher D. Timber for future? Attitudes towards timber construction by young millennials in Austria - Marketing implications from a representative study. J Clean Prod 2021;294:126324. https://doi.org/10.1016/j.jclepro.2021.126324.

[4] Sayigh A, editor. The Importance of Wood and Timber in Sustainable Buildings. Cham: Springer International Publishing; 2022. https://doi.org/10.1007/978-3-030-71700-1.

[5] Issa CA, Kmeid Z. Advanced wood engineering: glulam beams. Constr Build Mater 2005;19:99–106. https://doi.org/10.1016/j.conbuildmat.2004.05.013.

[6] Okamoto S, Akiyama N, Araki Y, Aoki K, Inayama M. Study on the strength of glued laminated timber beams with round holes: difference in structural performance between homogeneous-grade and heterogeneous-grade timber. J Wood Sci 2021;67. https://doi.org/10.1186/s10086-021-01941-3.

[7] Faircloth A, Gilbert BP, Kumar C, Leggate W, McGavin RL. Understanding the adhesion performance of glued laminated timber manufactured with Australian softwood and high-density hardwood species. Eur J Wood Wood Prod 2024;82:2013–28. https://doi.org/10.1007/s00107-024-02138-3.

[8] Falk RH, Colling F. Laminating Effects in Glued-Laminated Timber Beams. J Struct Eng 1995;121:1857–63. https://doi.org/10.1061/(ASCE)0733-9445(1995)121:12(1857).

[9] Wang Q, Wang Z, Feng X, Zhao Y, Li Z. Mechanical properties and probabilistic models of wood and engineered wood products: A review of green construction materials. Case Stud Constr Mater 2024;21:e03796. https://doi.org/10.1016/j.cscm.2024.e03796.

[10] Derkowski A, Kuliński M, Trociński A, Krzosek S, Mirski R. Selected Mechanical Properties of Glue-Laminated Timber Produced from Locally Repaired Timber. Materials 2022;15:8112. https://doi.org/10.3390/ma15228112.

[11] Kaya M. Physical and mechanical properties of laminated timbers used in the construction and furniture industry. BioResources 2024;19:6046–56. https://doi.org/10.15376/biores.19.3.6046-6056.

[12] Ehrhart T, Steiger R, Lehmann M, Frangi A. European beech (Fagus sylvatica L.) glued laminated timber: lamination strength grading, production and mechanical properties. Eur J Wood Wood Prod 2020;78:971–84. https://doi.org/10.1007/s00107-020-01545-6.

[13] Morin-Bernard A, Blanchet P, Dagenais C, Achim A. Glued-laminated timber from northern hardwoods: Effect of finger-joint profile on lamellae tensile strength.

Constr Build Mater 2021;271:121591. https://doi.org/10.1016/j.conbuildmat.2020.121591.
[14] Frese M, Blaß HJ. Characteristic bending strength of beech glulam. Mater Struct 2007;40:3–13. https://doi.org/10.1617/s11527-006-9117-9.
[15] Grazide C, Cointe A, Coureau J-L, Morel S, Dumail J-F. Wood heterogeneities and failure load of timber structural elements: a statistical approach. Wood Sci Technol 2015;49:421–40. https://doi.org/10.1007/s00226-015-0706-z.
[16] Guindos P, Guaita M. A three-dimensional wood material model to simulate the behavior of wood with any type of knot at the macro-scale. Wood Sci Technol 2013;47:585–99. https://doi.org/10.1007/s00226-012-0517-4.
[17] Zhang Y, Tian Y, Ding S, Lv Y, Samjhana W, Fang S. Growth, Carbon Storage, and Optimal Rotation in Poplar Plantations: A Case Study on Clone and Planting Spacing Effects. Forests 2020;11:842. https://doi.org/10.3390/f11080842.
[18] Gallego A, Ripoll MA, Timbolmas C, Rescalvo F, Suarez E, Valverde I, et al. Modulus of elasticity of I-214 young poplar wood from standing trees to sawn timber: influence of the age and stand density. Eur J Wood Wood Prod 2021;79:1225–39. https://doi.org/10.1007/s00107-021-01675-5.
[19] Rescalvo FJ, Timbolmas C, Bravo R, Gallego A. Experimental and Numerical Analysis of Mixed I-214 Poplar/Pinus Sylvestris Laminated Timber Subjected to Bending Loadings. Materials 2020;13:3134. https://doi.org/10.3390/ma13143134.
[20] Timbolmas C, Bravo R, Rescalvo FJ, Ringhofer A, Sieder R, Lorenzana J. Experimental study of hybrid pine-birch glued-laminated timber beams assisted by digital image correlation technique. Eur J Wood Wood Prod 2024;82:1187–99. https://doi.org/10.1007/s00107-024-02063-5.
[21] UNE-EN 1912. Structural Timber Strength classes Assignment of visual grades and species n.d.
[22] UNE 338_2016_Structural timber Strength classes n.d.
[23] Güray E, Kasal A, Demirci S, Ceylan E, Kuşkun T. Effects of cross-sectional geometry and force direction on bending strength and modulus of elasticity of some softwood beams. BioResources 2019;14:9258–70. https://doi.org/10.15376/biores.14.4.9258-9270.
[24] Fuentes-García Y. CARACTERIZACIÓN MECÁNICA DE CLONES DE CHOPO MC Y LUISA AVANZO Y SU VIABILIDAD PARA LAMINADOS ESTRUCTURALES. Universidad de Granada, 2025.
[25] Timbolmas C, Bravo R, Rescalvo FJ, Gallego A. Development of an analytical model to predict the bending behavior of composite glulam beams in tension and compression. J Build Eng 2022;45:103471. https://doi.org/10.1016/j.jobe.2021.103471.
[26] Gao Y, Wu Y, Zhu X, Zhu L, Yu Z, Wu Y. Numerical Analysis of the Bending Properties of Cathay Poplar Glulam. Materials 2015;8:7059–73. https://doi.org/10.3390/ma8105362.
[27] Gutiérrez Oliva A, Baonza Merino MV. Physical properties of wood of different clones of poplar, Zamora: 2001, p. 461–8.
[28] Martins C, Dias AMPG. Bending properties of LVL made by Eucalyptus globulus Labill. and its potential for hybrid glulam beams. Eur J Wood Wood Prod 2025;83:97. https://doi.org/10.1007/s00107-025-02244-w.

[29] Šuhajdová E, Schmid P, Novotný M, Pěnčík J, Šuhajda K, Uhlík O. Experimental Research on Hybrid Hardwood Glue-Laminated Beams. Buildings 2023;13:1055. https://doi.org/10.3390/buildings13041055.
[30] Fašalek A, Straže A, Šega B, Huber JAJ, Šernek M. Bonding Performance of Melamine–Urea–Formaldehyde and Polyurethane Adhesives for Laminated Hybrid Beams and Their Selected Mechanical Properties. Buildings 2023;13:2087. https://doi.org/10.3390/buildings13082087.
[31] Sciomenta M, Spera L, Peditto A, Ciuffetelli E, Savini F, Bedon C, et al. Mechanical characterization of homogeneous and hybrid beech-Corsican pine glue-laminated timber beams. Eng Struct 2022;264:114450. https://doi.org/10.1016/j.engstruct.2022.114450.
[32] Rescalvo FJ, Timbolmas C, Bravo R, Valverde-Palacios I, Gallego A. Improving ductility and bending features of poplar glued laminated beams by means of embedded carbon material. Constr Build Mater 2021;304:124469. https://doi.org/10.1016/j.conbuildmat.2021.124469.
[33] Riggio M, Anthony RW, Augelli F, Kasal B, Lechner T, Muller W, et al. In situ assessment of structural timber using non-destructive techniques. Mater Struct 2014;47:749–66. https://doi.org/10.1617/s11527-013-0093-6.
[34] Martins C, Dias AMPG, Cruz H. Blue gum: assessment of its potential for glued laminated timber beams. Eur J Wood Wood Prod 2020;78:905–13. https://doi.org/10.1007/s00107-020-01567-0.
[35] Timbolmas C, Bravo R, Rescalvo FJ, Portela M. Transformed-section method applied to multispecies glulam timber beams subjected to pure bending. Mech Adv Mater Struct 2022;29:6814–23. https://doi.org/10.1080/15376494.2021.1985665.
[36] UNE-EN_13183-1_2002_Moisture content of a piece of sawn timber Part 1: Determination by oven dry method n.d.
[37] Cirad. Non-destructive testing of wood. 2020. n.d.
[38] UNE 408-2011+A1_Timber structures_Structural timber and glued laminated timber _Determination of some physical and mechanical properties n.d.
[39] Khelifa M, Celzard A, Oudjene M, Ruelle J. Experimental and numerical analysis of CFRP-strengthened finger-jointed timber beams. Int J Adhes Adhes 2016;68:283–97. https://doi.org/10.1016/j.ijadhadh.2016.04.007.
[40] EN 12512:2001/A1:2005. EN 12512:2001/A1:2005. Timber Structures - Test methods - Cyclic testing of joints made with mechanical fasteners. 2005.
[41] Jorissen A, Fragiacomo M. General notes on ductility in timber structures. Eng Struct 2011;33:2987–97. https://doi.org/10.1016/j.engstruct.2011.07.024.
[42] UNE-EN 14080_Timber structures_Glued laminated timber and glued solid timber_Requirements n.d.
[43] UNE-EN Structural timber_ Determination of characteristic values of mechanical properties and density n.d.